Probabilistic stability and "tall" wind profiles: theory and method for use in wind resource assessment

Kelly, Mark C.; Troen, Ib

Published in:
Wind Energy

Link to article, DOI:
10.1002/we.1829

Publication date:
2016

Document Version
Peer reviewed version

WIND ENERGY
Wind Energ. 2014–2016; **00**:1–15
DOI: 10.1002/we

RESEARCH ARTICLE

Probabilistic stability and "tall" wind profiles: theory and method for use in wind resource assessment

Mark Kelly[1] and Ib Troen[1]

[1]Wind Energy Division/Meteorology Section, Risø Campus, Danish Technical University; Roskilde 4000 Denmark.

ABSTRACT

A model has been derived for calculating the effects of stability and the finite height of the planetary boundary layer upon the long-term mean wind profile. A practical implementation of this probabilistic extended similarity-theory model is made, including its incorporation within the European Wind Atlas (EWA) methodology for site-to-site application. Theoretical and practical implications of the EWA methodology are also derived and described, including unprecedented documentation of the theoretical framework encompassing vertical extrapolation, as well as some improvement to the methodology. Results of the modelling are shown for a number of sites, with discussion of the models' efficacy and the relative improvement shown by the new model, for situations where a user lacks local heat flux information, as well as performance of the new model using measured flux statistics. Further, the uncertainty in vertical extrapolation is characterized for the EWA model contained in standard (i.e. WAsP) wind resource assessment, as well as for the new model.

KEYWORDS

Atmospheric Stability; Monin-Obukhov similarity; Similarity theory; Wind profiles; Wind Extrapolation; Resource Assessment

Correspondence

e-mail: mkel@dtu.dk

Received . . .

1. INTRODUCTION

In order to provide better estimates of wind energy production at heights above the atmospheric surface layer ($z > \sim 50$ m), the extrapolation of measured statistics requires a model for the wind profile that is applicable over typical turbine lifetimes.*

Starting with Monin-Obukhov (M-O) similarity theory [1], models for the wind profile that include the effects of atmospheric stability have been accepted and employed for several generations. However, wind profile forms based on M-O theory are not expressly derived for application to wind characterization over the long-term (i.e. years), nor for use above the atmospheric surface layer. Power-law formulations are sometimes used for both 10-minute and long-term use in wind energy (e.g. [2], and implicit in the IEC standard [3]). However, these power-law forms lack any systematic or universal description of the connection or difference between short- and long-term wind profiles, and have only just begun to have useful theoretical or physical connection to geostrophic theory [4] and stability measures [5]. Swift&Dixon [6] did examine power-law exponent variation and connection to the log-law over the ocean, with some consideration of the effect of a z-dependent power law upon the Weibull parameters, but this was focused on the sea-induced speed-dependent roughness and subsequent change in Weibull shape. Two-layer models (which generally patch an Ekman-layer form above to some surface-layer form) have existed for some time (e.g. [7], [8], [9]), but have been generally idealized and not applied in wind energy; however, recently Optis *et al.* [10] examined the mean performance of the two-layer model of

*Though commercially available LIDAR devices can record wind speeds at these heights, LIDAR's costs still tend to be prohibitive, especially for longer (e.g. multi-year) measurement campaigns—which more reliably represent the local wind climate and reduce prediction uncertainties. Thus wind profile models are still needed for wind resource assessment, particularly on account of the ever-increasing hub heights (and rotor diameters) used in the wind industry.

Emeis *et al.* [11] in stable conditions. Kelly & Gryning [12] derived a statistical long-term wind profile model based on M-O theory by incorporating distributions of stability, then further generalized this probabilistic profile to extend the 'tall' profile model of [13] for use with long-term wind statistics. Here the label 'long-term' implies time scales on the order of several decades, i.e. the expected lifetime of a wind turbine.

The current *de-facto* standard for extrapolating measured winds for long-term wind energy predictions, contained within the European Wind Atlas ('EWA') [14] methodology implemented in software such as *'WAsP'*, does not explicitly specify a wind profile. Instead the EWA method calculates stability-induced deviations from the logarithmic wind profile, by applying perturbation theory to both the M-O form for the wind profile and to the geostrophic drag law. In effect the EWA framework for extrapolating winds includes a local or 'micro-scale' component, operating on wind statistics observed at a single location, as well as a larger-scale (geostrophic) part in its modeling. The EWA method uses this prescription for long-term wind variance also, to give a coupled formulation for the extrapolation of both wind speed and Weibull shape parameters—and subsequently wind energy density [15]—affected by geostrophic-scale stability perturbations.

In this paper we adapt and augment the long-term wind profile model of Kelly & Gryning [12] to function within the EWA framework [14]; i.e. we modify the presumably micro-scale profile to account for geostrophic-scale influences. We also show how the probabilistic profile of [12] (or potentially other scalar wind profile forms) can be made consistent with the geostrophic basis of the EWA, for practical modeling of the profiles of wind statistics. This includes elaboration of theoretical details of the EWA methodology as well as some further refinement of the method, outlining both theoretical and practical consequences of its use and adaptation.

2. THEORY, DEVELOPMENT, AND MODELING

We use the assumption that wind speed observations U, when averaged over a period of 10–30 minutes (typical in wind energy) and taken over sufficiently narrow wind sectors (typically $\leq\sim 30^\circ$) over one or more years, have a probability distribution function (PDF) described by a two-parameter Weibull form

$$p(U) = \frac{k}{U}\left(\frac{U}{A}\right)^k \exp\left[-\left(\frac{U}{A}\right)^k\right] \tag{1}$$

with scale parameter A and shape parameter k. For a wind speed probability distribution of the Weibull form (1), the n^{th} moment of the wind speed is given by

$$\langle U^n \rangle (z) = [A(z)]^n \, \Gamma\{1 + n/k(z)\} \tag{2}$$

where angle-brackets denote an average over one or more years, and $\Gamma\{x\}$ is the Gamma function. So the profile of long-term mean wind speed is $A(z)\Gamma\{1 + 1/k(z)\}$; its height dependence is predominantly contained in the scale parameter profile $A(z)$, though a non-negligible contribution from $k(z)$ can affect the vertical variation of wind power density via profiles of higher moments of wind speed [15, 16].

2.1. Long-term probabilistic wind speed profile

As a statistical extension of Monin-Obukhov similarity theory, [12] derived the profile of long-term dimensionless mean wind speed, based on their universal form for observed dimensionless stability distributions. The latter was derived as a two-sided probability density of inverse Obukhov length L^{-1} for stable and unstable conditions, which we denote by subscripts "+" ($L^{-1} > 0$) and "−" ($L^{-1} < 0$) respectively:

$$P(L^{-1}) = n_\pm \frac{C_\pm}{\sigma_\pm} \frac{\exp\left[-\left(C_\pm |L^{-1}|/\sigma_\pm\right)^{2/3}\right]}{\Gamma[5/2]}. \tag{3}$$

The (inverse) Obukhov length is defined here as $L^{-1} = -\kappa(g/T_0)H_{\text{sfc}}/u_{*0}^3$, i.e. through the kinematic flux of virtual temperature $H_{\text{sfc}} = \overline{wT_v}$ (i.e. heat flux per mass, accounting for humidity), friction velocity $u_{*0} \equiv [(\overline{uw})^2 + (\overline{vw})^2]^{1/4}$, and temperature T_0 in the surface layer,[†] with g=9.8 m s^{-2} the gravitational acceleration and κ=0.4 the von Kármán constant. Here $\{n_+, n_-\}$ are the respective fractions of occurrence of stable and unstable conditions, which together with $C_\pm/\sigma_\pm\Gamma(5/2)$ in (3) ensure that $\int_{-\infty}^{\infty} P(L^{-1})\mathrm{d}L^{-1} = 1$. The scale parameters $\{\sigma_+, \sigma_-\}$ are representative magnitudes

[†]These quantities can be measured using e.g. a three-dimensional (or 2-D) sonic anemometer within the atmospheric surface layer (below 1/10th of the atmospheric boundary layer depth, which can be shallower than 200 m at night), typically taken from a height of 10 m and averaged over 10–30 minutes. Averaging times shorter than 10 minutes should not be used (c.f. [17]).

Wind Energ. 2014–2016; **00**:1–15 © 2014–2016 John Wiley & Sons, Ltd.
DOI: 10.1002/we
Prepared using weauth.cls

of variations in L^{-1} observed in the atmospheric surface layer over the course of years (here 'observed' connotes time averages generally taken over 10–30 minutes), for each side of the distribution (i.e. stability regime); they are proportional to the width of the L^{-1} distribution for stable and unstable regimes, respectively. The $\sigma_\pm$ are found as in [12] via the long-term standard deviation of the heat fluxes $\{H_+, H_-\}$ and mean friction velocity $\langle u_{*0}\rangle$, for stable and unstable conditions, respectively:

$$\sigma_\pm = \frac{g}{\rho c_p T_0} \frac{\left\langle (H - \langle H\rangle_\pm)^2 \right\rangle_\pm^{1/2}}{\langle u_{*0}\rangle_\pm^3}\,, \tag{4}$$

where $\langle\rangle_\pm$ denotes an average taken (separately) over either stable or unstable conditions. The stability variability parameters $\sigma_\pm$ can thus be calculated from (4) via observed mean friction velocity and r.m.s. heat flux under stable and unstable conditions, respectively.[‡] We note that *temperature gradients cannot be relied upon for this purpose*, as they do not reliably give universal stability distributions (c.f. [12]); among other issues, temperature signals measured at significantly different heights tend to fall within the surface layer for different proportions of time over the long term, and have statistically different behavior (see e.g. [18]). We also re-iterate the finding of [12] that it is the *widths* of the stable and unstable distributions which moderate the long-term wind profile, thus attempting to define some 'mean stability' ($1/\langle L\rangle$ for example) *is not useful* without more information.

[12] further generalized and adapted the 'tall' wind profile of [13]—which includes the effect of atmospheric boundary-layer depth h through height-varying friction velocity $u_*(z/h)$ and geostrophic wind speed $G = U|_{z=h}$—to a climatological-mean form usable for wind resource estimates. The distribution (3) facilitated finding such a form for the mean wind profile. Using representative values $h_{\rm eff}$ and geostrophic wind speed $G_{\rm eff}$ (as well as a mean roughness z_{0m}, which is done implicitly but without acknowledgement in most wind resource estimates), then integrating the product of $P(L^{-1})$ and the wind profile over L^{-1} approximates the ensemble-mean of the "tall" wind profile. Integrating the product of U/u_{*0} and $P(L^{-1})$ over L^{-1} (using a generalized version of [13]'s profile for U/u_{*0}) produces [12]

$$\begin{aligned}\left\langle \frac{kU}{u_{*0}} \right\rangle (z; z_{0m}, \sigma_\pm, h_{\rm eff}, G_{\rm eff}) = \ln\left(\frac{z}{z_{0m}}\right) - \langle\psi\rangle(z) - \frac{z}{h_{\rm eff}}\left[\overline{\langle\psi\rangle_z} - \langle\psi\rangle(z)\right] \\ + \frac{h_{\rm eff}}{2\ell_{\rm mid}^{\rm eff}}\left[1 - \left(1 - \frac{z}{h_{\rm eff}}\right)^2\right] + \frac{z}{h_{\rm eff}}\left(s_{\rm eff} - 1\right)\end{aligned} \tag{5}$$

where u_{*0} is the surface-layer friction velocity, $\overline{\langle\psi\rangle_z} \equiv z^{-1}\int_{z_0}^{z}\langle\psi\rangle(z)dz$ is the long-term stability correction averaged up to height z, and $s_{\rm eff} \equiv k h_{\rm eff}\langle u_{*0}^{-1} dG/dz\rangle$ is the mean dimensionless ABL shear.[§] To get (5) we have defined the effective climatological (mean) geostrophic wind speed $G_{\rm eff}$ as the corresponding mean wind speed evaluated at the effective ABL depth, $G_{\rm eff} = \langle U\rangle|_{h_{\rm eff}}$. Essentially $h_{\rm eff}^{-1}$ is the long-term mean inverse ABL depth, which is somewhat biased by stable conditions so that $h_{\rm eff} \sim$300–500 m, consistent with the distributions $P(h)$ given by [20] (c.f. also [15]).

Compared with a logarithmic profile, the mean profile (5) consists of the Monin-Obukhov ("M-O") profile [21] in climatological form (log-law with mean stability correction $\langle\psi\rangle$), plus terms representing the combined effect of stability and height-dependent friction velocity $u_*(z/h)$, a 'matching' term which helps to drive $\langle U\rangle$ towards $G_{\rm eff}$ as $z \to h_{\rm eff}$, and a geostrophic shear term (which can be due to e.g. large-scale horizontal temperature gradients, i.e. thermal wind). The matching coefficient $h_{\rm eff}/2\ell_{\rm mid}^{\rm eff}$ is the difference between $\kappa G_{\rm eff}/\langle u_{*0}\rangle$ and the vertically averaged dimensionless M-O profile evaluated at $h_{\rm eff}$, minus the geostrophic shear contribution [12]:

$$\frac{h_{\rm eff}}{2\ell_{\rm mid}^{\rm eff}} \simeq \frac{\kappa G_{\rm eff}}{u_{*0}} - \left[\ln(h_{\rm eff}/z_{0m}) - h_{\rm eff}^{-1}\int_{z_0}^{h_{\rm eff}}\langle\psi\rangle(z)dz\right] - (s_{\rm eff} - 1)\,. \tag{6}$$

For simplicity and consistency with the value implicit in the original 'tall' profile form of [13],we take the effective long-term dimensionless geostrophic shear to be unity, $s_{\rm eff} = 1$; thus the last term of (5) vanishes, as does the corresponding $s_{\rm eff}$ contribution to $\ell_{\rm mid}$ in (6).

The use of (3) also led to a probabilistic long-term mean stability correction in (5), of the form

$$\langle\psi\rangle(z) = -n_+\frac{3\sigma_+}{C_+}b'z \quad + \quad n_- f_-\left(\frac{\sigma_-}{C_-}\beta z\right). \tag{7}$$

[‡] Over land one can use $\langle u_{*0}\rangle_\pm \simeq \langle u_{*0}\rangle$ without breaking it into separate means for stable and unstable conditions, because doing so has a minor effect on $\sigma_\pm$ in most situations—as noted by [12], who also state that the $\sigma_\pm$ are defined as in (4) avoiding parameters based on L^{-1} (e.g. moments of L^{-1}), because the latter can be relatively biased by the tails of the L^{-1}-distribution (where M-O similarity fails to apply) and thus reduce the applicability of (3).

[§] Note that [12] contains a typographical error in the definition of s, which was limited there to baroclinic shear; the error was introduced after article proofing. The ABL shear (s or $s_{\rm eff}$) can contain a baroclinic contribution (due to large-scale horizontal temperature gradients), as well as contributions from e.g. surface inhomogeneities or terrain (see e.g. [19]).

Here $b' \equiv b/\Gamma\,(5/2) \simeq 0.75b$ and $b \simeq 4.7$ is the conventional M-O stability correction coefficient for stable conditions, and the mean unstable correction function f_- is derived from the classical form $\psi(z/L)$ (via integration over all unstable states $L < 0$, see [12]).

For practical use, because of the dominance of the stable-contributions, for $n_+ > 0.1$ (i.e. stable conditions occurring at least 10% of the time, which is rarely ever violated) we recommend approximating the vertical-mean correction in (5) by

$$\overline{\langle\psi\rangle_z} = z^{-1}\int_{z_0}^{z}\langle\psi\rangle(z')dz' \approx \langle\psi\rangle(z/2). \tag{8}$$

We also suggest using a 'default' value of $\ell_{\rm mid}^{\rm eff} = h_{\rm eff}/2$, consistent with the findings reported in [13] and noting further that the term with this coefficient has the weakest z-dependence of the three correction terms in (5); furthermore, this weak z-dependence can also change character if the friction velocity profile $u_*(z/h)$ is prescribed differently (e.g. if u_*^2 is made to be linear in z/h). We also use the approximation for the mean unstable correction noted in the Appendix of [12]:

$$f_-\left(\frac{\sigma_-}{C_-}\beta z\right) \approx \psi_-\left(\frac{z}{L_{\rm equiv}}\right), \qquad L_{\rm equiv} \equiv (-0.4\sigma_-)^{-1} \tag{9}$$

where

$$\psi_-(\xi) = \frac{\pi}{\sqrt{3}} + \frac{3}{2}\ln\left\{\frac{1}{3}\left[1 + x^{1/3} + x^{2/3}\right]\right\} - \sqrt{3}\,\tan^{-1}\left[\frac{1+2x^{1/3}}{\sqrt{3}}\right], \qquad x \equiv (1-\beta\xi) \tag{10}$$

is the Monin-Obukhov stability correction function that gives the appropriate behavior in the limit of free convection, with $\beta \simeq 12$ (as in e.g. Carl *et al.* [22]).

Using (8) and the approximations above including a 'default' $\ell_{\rm mid}^{\rm eff} = h_{\rm eff}/2$, a practical ('user-friendly') form of the long-term dimensionless wind profile (5) can be written as

$$\left\langle\frac{kU}{u_{*0}}\right\rangle(z) \simeq \ln\left(\frac{z}{z_{0m}}\right) - \langle\psi\rangle(z) - \frac{z}{h_{\rm eff}}\left[\langle\psi\rangle(z/2) - \langle\psi\rangle(z)\right] + \frac{z}{h_{\rm eff}}\left(2 - \frac{z}{h_{\rm eff}}\right), \tag{11}$$

where from (7) and (9) the corresponding climatological stability function is approximately

$$\langle\psi\rangle(z) \simeq -10.6 n_+ z\sigma_+ + (1-n_+)\psi_-(-0.4z\sigma_-) \tag{12}$$

with ψ_- again given by (10). The simplified long-term stability correction (12) tends to be dominated by the stable-side correction, which is proportional to height z, σ_+ (variability of L^{-1} in stable conditions), and the fraction of conditions at a site which are stable, n_+. The unstable component ψ_- is positive and increases monotonically with height, but weaker than linear in z. Thus in the wind profile (e.g. Eqn. 11) the stability correction tends to have a stable contribution which increases the shear and wind with height, plus a weaker unstable contribution which opposes this; basically the end result is a climatological wind profile which has higher shear than the log-law over most of the ABL, but which also has decreasing shear as the effective (climatological) ABL 'top' ($h_{\rm eff}$) is approached. The climatological stability correction and dimensionless wind profile are discussed and shown in more detail in [12].

2.2. European Wind Atlas Method

The European Wind Atlas methodology [14] exploits the assumption that observation and prediction sites share the same geostrophic wind G (forcing, in a nonlocal statistical-mean sense), and models the effects of geostrophic-scale surface heat flux through perturbation theory. That is, the EWA method does large-scale (non-local, geostrophic) perturbation of (locally) observed wind statistics in its treatment of stability and vertical extrapolation. The height (z_m) of minimum stability-induced wind deviations is determined from geostrophic theory (see Eqn. A.10 in Appendix), and the Monin-Obukhov (M-O) wind profile—which is originally valid on a local, microscale level—is perturbed around z_m. The perturbations have essentially two kinds of contributions. First, the M-O form for wind speed is evaluated at z_m, and has two components in its climatological stability correction: one due to fluctuations in surface heat flux (Obukhov length via rms value $H_{\rm rms}$), and an "offset" piece due to stable conditions having a mean dominating effect on the wind shear (via $L_{\rm off}^{-1} \propto H_{\rm off}$). The second type of contribution to the perturbed M-O form consists of geostrophic-scale stability-induced perturbations of friction velocity, for a given forcing (derived from surface heat flux perturbations, see Appendix); these also include both an rms and offset component.

The EWA's total stability contribution to (perturbation of) the logarithmic wind profile for a given site and height z above the surface can be written simply as

$$\left(\frac{z}{z_m}\right)\left[\Delta u_{*\rm rms}\ln\left(\frac{z_m}{z_0}\right) - \psi\left(\frac{z_m}{L_{\rm off}}\right) - \psi\left(\frac{z_m}{L_{\rm rms}}\right)\right] + \Delta u_{*\rm off}\ln\left(\frac{z}{z_0}\right), \tag{13}$$

Wind Energ. 2014–2016; **00**:1–15
DOI: 10.1002/we
Prepared using weauth.cls

i.e. the mean wind at height z is comprised of the sum of (13) and the logarithmic 'base' profile $U_0(z) \equiv u_{*0}\kappa^{-1}\ln(z/z_0)$. We also point out that for z_0 the EWA uses a geostrophic-scale roughness, which for a given direction is calculated upwind via weighted averages [14].[¶] Normalizing (13) by U_0 for a given site, we obtain the dimensionless perturbation p', which expresses the relative effect of stability on the mean wind. A mean wind "correction factor" $\mathtt{cf}_1$ can be defined as the ratio of scaling factors at target ('receiver') and measurement ('source') sites, allowing calculation of the mean wind at height $z_{\rm rec}$ over roughness $z_0^{\rm rec}$ from the wind measured at $z_{\rm src}$ over $z_0^{\rm src}$, i.e. via $\langle U_{\rm rec}/U_{0,\rm rec}\rangle = \mathtt{cf}_1\langle U_{\rm src}/U_{0,\rm src}\rangle$; this is indeed e.g. how the industry-standard software WAsP finds $\langle U(z_{\rm rec}, z_0^{\rm rec})\rangle$ from $\langle U(z_{\rm src}, z_0^{\rm src})\rangle$ (after accounting for variations in roughness and terrain elevation). The correction factor for wind can thus be expressed as

$$\mathtt{cf}_1 = \frac{1 + p'(z_{\rm rec}, z_0^{\rm rec}, H_{\rm off}, H_{\rm rms}, G)}{1 + p'(z_{\rm src}, z_0^{\rm src}, H_{\rm off}, H_{\rm rms}, G)}. \tag{14}$$

The EWA [14] used a perturbation of the geostrophic drag law around its basic form for neutral conditions to first order in (u_*/fL) to obtain a relationship between perturbations $\mathrm{d}u_*$ and $\mathrm{d}H$ (see A.6 for full derivation); it then separates heat flux contributions into a mean 'offset' component $H_{\rm off}$ and a fluctuating component $H_{\rm rms}$, which subsequently give a $\Delta u_{*\rm off}$ and $\Delta u_{*\rm rms}$. Using the expressions for du_* developed in the Appendix to write $\{\Delta u_{*\rm off}, \Delta u_{*\rm rms}\}$ in terms of $\{H_{\rm off}, H_{\rm rms}\}$ and dividing (13) by U_0, the dimensionless stability perturbation can be written compactly as $p'\,(z, z_0, G, f, H_{\rm off}, H_{\rm rms})$, i.e. for a given site

$$p' = \frac{z/z_m}{\ln(z/z_0)}\left[a_G\frac{C_{\rm rms}H_{\rm rms}}{fG^2}\ln\left(\frac{z_m}{z_0}\right) - \psi_W\,(z_0, H_{\rm off}, H_{\rm rms}, G, f)\right] + a_G\frac{H_{\rm off}}{fG^2}. \tag{15}$$

Here we abbreviate $\psi_W \equiv \psi(z_m/L_{\rm off}) + \psi_-(z_m/L_{\rm rms})$ as the effective stability function, and remind that z_m actually depends on $\{z_0, G, f\}$. The fluctuating contribution is modeled by the EWA through an unstable correction function $\psi_-(z_m/L_{\rm rms})$, where $L_{\rm rms}$ is the Obukhov length corresponding to $C_{\rm rms}H_{\rm rms}$ (since $H_{\rm rms} \geq 0$), and $C_{\rm rms}$ is a constant prescribed by [14] to be 0.6.[‖] The offset (mean) component of ψ_W depends on $H_{\rm off}$ through $L_{\rm off}^{-1}$, and the EWA-recommended (WAsP default) over-land value of $H_{\rm off} = -40\,\mathrm{W\,m^{-2}}$ leads to a stable contribution $\psi_+(z_m/L_{\rm off})$ to ψ_W (if $H_{\rm off} > 0$ is chosen, then the unstable form $\psi_-(z_m/L_{\rm off})$ is used in in Eqs. 13 and 15). The ψ are calculated using Monin-Obukhov similarity functions [23], with Obukhov length L defined using the respective offset and rms heat fluxes, along with the geostrophic-scale friction velocity. The latter is approximated by the EWA through the wind speed ($U_{\rm mpd} \equiv A(1+2/k)^{1/k}$) corresponding to maximum available power density from observed (input) Weibull parameters, along with an assumed logarithmic profile for this statistic ($u_* = \kappa U_{\rm mpd}/\ln(z_{\rm obs}/z_0)$), again using the geostrophic (averaged upwind) roughness z_0; see [14] for more details. The geostrophic wind speed can then be obtained from the geostrophic drag law

$$\frac{\kappa G}{u_*} = \sqrt{\left[\ln\left(\frac{u_*/f}{z_0}\right) - A_0^2\right] + B_0^2}, \tag{16}$$

where A_0 and B_0 are the neutral barotropic geostrophic drag coefficients, taken to be 1.8 and 4.5, respectively [14].

The last term in the EWA non-dimensional wind perturbation (15) is independent of height, and represents the perturbation $\Delta u_*/u_*$ in near-surface geostrophic-scale friction velocity (u_*) due to surface-based stability contributions to the geostrophic balance, with $a_G \equiv 2.5g/(\rho c_p T_0)$[**] arising from the definition of L. Note also that in (15) we have absorbed the functional dependences of $z_m(z_0, G, f)$ and $u_*(z_0, G, f)$ into ψ_W, to show with (13) that the EWA stability model gives only a *linear height dependence* of dimensional stability contributions to mean wind speed—the height z appears only in front of the bracketed term of (15). One can also see from (15) that $H_{\rm off}$ has a larger influence on the EWA stability correction than $H_{\rm rms}$, particularly over land where $H_{\rm off}$ is negative; this parameter tends to be the primary one dictating (the shear in) WAsP's vertical extrapolation.

[¶] The European Wind Atlas (EWA) finds the geostrophic roughness upwind by geometric average (equivalent to averaging the logarithms of roughnesses), with weighting function $\exp(-r/\ell_r)$ for distance r upwind. The e-folding distance ℓ_r is suggested to be 10 km [14] (which is the default value prescribed in e.g. WAsP).

[‖] The factor $C_{\rm rms}$ leads to an *effective* EWA-recommended rms heat flux of 60 W/m^2, from $C_{\rm rms}H_{\rm rms} = 0.6\times 100\,\mathrm{W/m^2}$. The EWA-recommended (WAsP default) value of $H_{\rm rms}$=100 W/m^2 appears directly only in the perturbation of wind-speed variance, which is used for calculation of the Weibull-k profile; see [15]. Further, implementations of the EWA (e.g. WAsP 9–10) also include a damping coefficient $\exp[(-z/h_g)^{1.5}]$ multiplying the bracketed term in eqns. (13) and (15); however, the damping height h_g is large enough that $\mathtt{cf}_1$ is not significantly affected, even at heights z up to 250 m.

[**] If $\{H_{\rm off}, H_{\rm rms}\}$ are given in W m^{-2}, an additional factor $(\rho c_p)^{-1}$ appears; ρ and c_p are the surface-layer air-density and constant-pressure heat capacity.

2.3. Adaptation of statistical 'tall' profile to EWA framework

The long-term dimensionless profile (5) can be translated into an effective profile correction factor, i.e. expressed as perturbation-like form, by normalizing it with the neutral 'uncorrected' log-profile:

$$\mathtt{cf}_1(z_{\rm src}, z_{\rm rec}) = \frac{\left[\left\langle kU(z,h,L,z_0)/u_{*0}\right\rangle_{L,h,z_0,G} \Big/ \ln(\frac{z}{z_{0\rm eff}})\right]\Big|_{\rm rec}}{\left[\left\langle kU(z,h,L,z_0)/u_{*0}\right\rangle_{L,h,z_0,G} \Big/ \ln(\frac{z}{z_{0\rm eff}})\right]\Big|_{\rm src}} = \frac{1+p'_T(z,z_{0_{\rm eff}},\sigma_\pm,n_+,h_{\rm eff},G)_{\rm rec}}{1+p'_T(z,z_{0_{\rm eff}},\sigma_\pm,n_+,h_{\rm eff},G)_{\rm src}}, \qquad (17)$$

which is again a ratio taken from observation to prediction sites that share a wind climate (G), with the 'tall' long-term stability model for normalized deviations from the logarithmic profile (i.e. from eq. 11) denoted by p'_T. The dependence of $\langle U\rangle$ upon $\{z_{0m}, \sigma_\pm, n_+, h_{\rm eff}, \ell^{\rm eff}_{\rm mid}\}$ is suppressed hereafter for notational simplicity.

2.3.1. Adaptation for use with geostrophic drag-law.

In order to use the probabilistic profile theory within the context of wind resource assessment, however, one must connect the statistics from a given observation site and the site of application, while accounting for the relevant differences between sites. Thus again the stability-induced long-term mean shift in geostrophic friction velocity needs to be treated (i.e. stable conditions affect u_* for a given G), meaning the normalized dimensionless profile $\langle kU(z)/[u_{*0}\ln(z/z_0)]\rangle$ will need to be multiplied by a factor $(1+\Delta u_{*\rm off}/u_{*0})$; since in practice the perturbation ($a_G H_{\rm off}/fG^2$, as seen in eq.15) is much smaller than 1, and because the the other normalized perturbations are relatively small, for the new 'tall' profile we approximate by adding $a_G H_{\rm off}/fG^2$ to p'_T in (17). Figure 1 shows the correction factor (17) as a function of target height, i.e. the dimensionless wind profile, for the case of observations taken at 40 m height, with stability statistics typical of those found from measurements at flat mid-latitude sites [12]: σ_+ =0.007 m^{-1}, n_+ =0.6 (i.e. negative heat flux or stable conditions 60% of the time), σ_- =0.04 m^{-1}, and effective ABL depth of $h_{\rm eff}$ =400 m over surface roughness length $z_{0,\rm rec} = z_{0,\rm src}$=3 cm. One can see from the figure that these values in effect correspond to the empirically determined values used by the EWA formulation, including the geostrophic 'offset' heat flux of $H_{\rm off}$=40 Wm^{-2}. One can see from Figure 1 how the new tall model diverges from the EWA model above ∼150 m; this is due to the 'tall profile' accounting for the effect of the ABL depth, and it prevents the new model from over-predicting winds far above the surface layer.

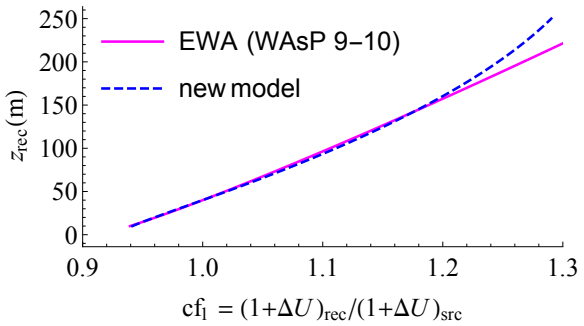

Figure 1. Profile of mean wind speed correction factor (dimensionless wind profile) $\mathtt{cf}_1(z)$ for source and target sites, via EWA (magenta) and new tall (blue/dashed) model (17). Observation height is $z_{\rm src}$ =40 m and corresponding roughness length is $z_{0,\rm src}$ =3 cm; here with typical stability statistics $\{\sigma_\pm, n_+, h_{\rm eff}\}$ and suggested EWA parameters $\{H_{\rm off}, H_{\rm rms}\}$.

2.3.2. Adaptation for application over different roughnesses; consistency with geostrophic drag law.

Since the probabilistic dimensionless profile in (11) (and [12]) was not derived with regard to application within the context of the geostrophic drag law, its mean stability function lacks the effect of a roughness-dependent geostrophic friction velocity, as in (16). Simply using the profile correction factor (17), based on the probabilistic profile form (11), will result in an improper scaling of wind speed when using observation and target locations with different roughnesses; in fact, the z_0-dependence of $\mathtt{cf}_1$ will be dominated by $[\ln(z/z_0)]-1$, giving the opposite trend than observed in reality. Invoking a scale-separation argument (the geostrophic scales are much larger than the footprint of surface heat fluxes), the 'missing' geostrophic friction velocity dependence can be put into $\langle\psi\rangle$, knowing that $L^{-1} \propto u_*^{-3}$. Because the stable side dominates the stability correction, a simple model is to multiply $L^{-1}|_+$—and thus $\langle\psi\rangle_+$—by $[u_*(z_0)/u_*(z_{0s})]^{-3}$, where $u_*(z_{0s})$ is simply a reference friction velocity, equal to the (minimum) geostrophic friction velocity (i.e. $G(z_{0s})$ via Eq. 16) occurring over sea roughness z_{0s}. Accounting for this, the new model profile can be expressed as p'_T and cast in a way to allow comparison with the accepted EWA form (15):

$$p'_T = \frac{z/h_{\rm eff}}{\ln(z/z_0)}\left[\frac{-\langle\psi\rangle_G(z)}{z/h_{\rm eff}} + \langle\psi\rangle_G(z) - \langle\psi\rangle_G(z/2) + \frac{h_{\rm eff}}{2\ell_m}\left(2-\frac{z}{h_{\rm eff}}\right)\right] + a_G\frac{H_{\rm off}}{fG^2}. \qquad (18)$$

Wind Energ. 2014–2016; **00**:1–15 © 2014–2016 John Wiley & Sons, Ltd.
DOI: 10.1002/we
Prepared using weauth.cls

Here in (18) using (7) and (9–10) with $C_\pm$ from [12], we have

$$\langle\psi\rangle_G \equiv -10.6 n_+ \sigma_+ z \left[\frac{u_*(z_0)}{u_*(z_{0s})}\right]^{-3} + n_-\psi_-(-0.4\sigma_- z) \tag{19}$$

denoting the probabilistic stability function modified to account for having different roughness lengths at observation and prediction sites, when relating via $G_{\rm src} = G_{\rm rec}$. The factor (18) is normalized as in the perturbation-form stability corrections employed by WAsP [14]. Figure 2 shows the effective roughness dependence of the adapted tall-profile treatment, along with the EWA behaviour. One can see from the figure that the model incorporating the geostrophic-

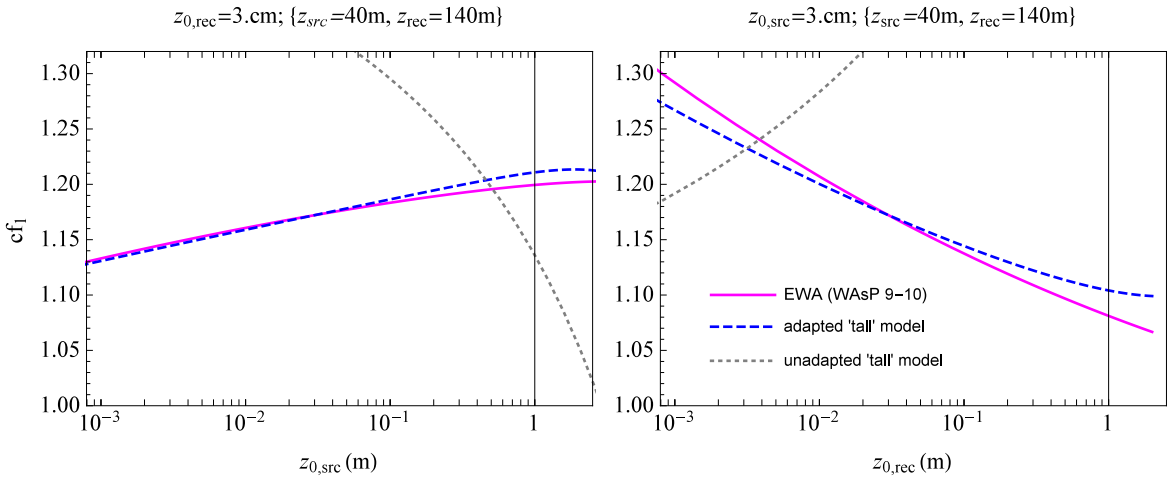

Figure 2. $\mathtt{cf}_1$ as function of roughness length, for EWA (magenta) and new (blue) model including geostrophic $u_*(z_0)$ dependence (19). Left: for varying observation-site geostrophic roughness $z_{0\rm src}$, given a receiver site $z_{0\rm rec}$=10 cm; right: as a function of target site geostrophic roughness $z_{0\rm rec}$, given an observation site roughness of 3 cm. Both are for receiver (target) height of $z_{\rm rec}$ =140 m, given an observation (source) height of $z_{\rm src}$ =40 m. Black/dotted lines: using (12) for $\langle\psi\rangle$, without geostrophic adaptation.

scale roughness effect on friction velocity into the new stability treatment (19) produces a very similar z_0-dependence in predicted mean wind speed compared to the EWA. Neglecting such a dependence would in effect render the new statistical profile treatment incompatible with application of the geostrophic drag law at two sites; this is shown by the black dotted lines in Figure 2, which show $\mathtt{cf}_1(z_0)$ using (12) for $\langle\psi\rangle$ instead of its geostrophic-adapted form (19).

We further see that for the profile to be consistent with the geostrophic drag law, then G/u_* from (16) should be consistent with the coefficient of the geostrophic-matching term,

$$\frac{h_{\rm eff}}{2\ell_{\rm eff}} \simeq \frac{kG}{u_{*0}} - \ln(h_{\rm eff}/z_0) + h_{\rm eff}^{-1}\int_{z_0}^{h_{\rm eff}} \langle\psi\rangle(z)dz, \tag{20}$$

which is observed to be of order 1 (e.g. [12, 13]). Such a value—and consistency with the geostrophic drag law—is only possible when setting $\langle\psi\rangle = \langle\psi\rangle_G$, i.e. including the u_* dependence as in (19). Otherwise, unreasonably large magnitudes of the $h_{\rm eff}/2\ell_{\rm eff}$ 'matching' term ensue.

3. VALIDATION AND RESULTS

Self-predictions of wind speed employing both the EWA model and the adapted new model were made at a total of 8 onshore and 5 offshore sites, with each site having observations at numerous measurement heights. Four of the offshore sites are located around the North Sea and use LIDAR (Siri, TAQA platform, Utsira, Schooner, see [24]), with one offshore site (Stora Middelgrund) located between Sweden and Denmark; the microscale winds of all offshore sites are unaffected by coasts. One land site, Østerild, uses LIDAR data; the LIDAR is located in an extended clearing within a limited forest, but we use only measurements higher than twice the mean tree height in order to avoid the forest-induced roughness sublayer and also related distortion of the LIDAR measurements [25]. All of the land sites are in relatively flat terrain;

Høvsøre, Ferrel, and Risø are affected by a coastline[††], while the others have relatively insignificant roughness changes. The Hamburg data is for the sectors in a suburban environment, as discussed in [12]. An integer number of years of data, consisting of 10-minute mean winds and directions, were used from each site; each dataset has a recovery rate greater than 90%, with only randomly distributed gaps. The sites used in this study are listed in Table I.

Site	type	measurement heights (m)
Høvsøre	coastal	10, 60, 100, 116.5
Hamburg	suburban	10, 50, 110, 175, 250
Cabauw	flat land	20, 40, 80, 140, 200
Ferrel	flat land	10, 30, 100
Risø	flat land	27, 43, 76, 117
Sprogø	offshore	18, 55, 68
Kivenlahti	∼uniform forest	21, 92, 224
Østerild	forest (lidar)	45,60,80,100,120,140,170,200
Schooner	offshore (lidar)	76,92,99,102,107,116,126,152,182,216
Siri	offshore (lidar)	85,105,125,145,161,175,205
Stora Middelgrund	offshore	20,60,92,117
TAQA	offshore (lidar)	70,90,110,130,150,170,190,210
Utsira	offshore (lidar)	40,53,73,93,113,133,153,173

Table I. Sites and measurement heights used for vertical extrapolation study.

3.1. Extrapolation without flux observations

Results of our vertical extrapolation calculations are given in Figure 3, which shows the mean absolute error for upward extrapolations as a function of relative extrapolation distance $\ln(z_{\rm rec}/z_{\rm src})$; the error, i.e. difference between predictions and measurements at heights $z_{\rm rec}$, is given for both the EWA model (blue, using standard WAsP settings for its stability treatment, as below Eq.15) as well as the new model (red). The mean is calculated for 'bins' of $\ln(z_{\rm rec}/z_{\rm src})$, where all of the sites' data have been aggregated together. The ranges of $\ln(z_{\rm rec}/z_{\rm src})$ have been chosen so that each bin contains approximately the same number of results (∼10), in order to avoid introducing an artificial $(z_{\rm rec}/z_{\rm src})$ dependence in the extrapolation error. The standard deviation per bin is also indicated by the vertical bars in the plot. For this first validation

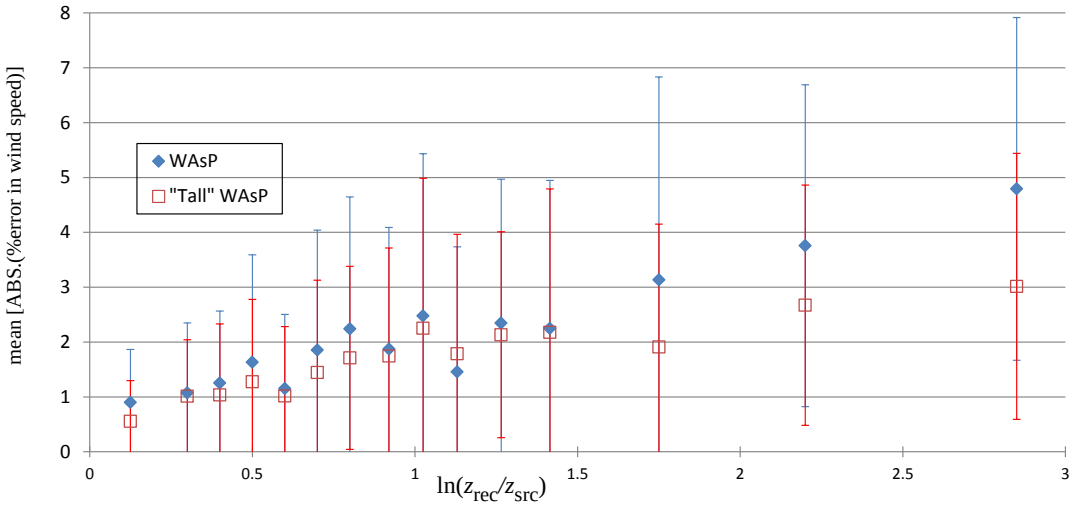

Figure 3. Mean of absolute error in climatological wind speed extrapolation per 'bin' of relative extrapolation $\ln(z_{\rm rec}/z_{\rm src})$, where each bin has the same number of samples.

comparison, in the new model we used values of the stability variability parameters $\sigma_\pm$ and $n_\pm$ that correspond to the

[††]Note at Risø there is a narrow, shallow fjord affecting the mast, but only for a narrow range of wind directions.

Wind Energ. 2014–2016; **00**:1–15 © 2014–2016 John Wiley & Sons, Ltd.
DOI: 10.1002/we
Prepared using weauth.cls

recommended EWA (default WAsP) parameter values of $\{H_{\rm off}, H_{\rm rms}\}$ (as in Figs. 1–2), and with effective ABL depths of 400 m and 250 m (for terrestrial and off-shore sites, respectively).[‡‡] This was done because it is the 'default' method, i.e. the settings most likely employed by a wind assessment engineer lacking any stability information (below we treat cases using measured stability statistics). Note the predictions shown in Fig. 3 include minor terrain effects due to the inclusion of the EWA (WAsP) models for roughness and terrain elevation changes; this was done to evaluate the models' performance in the most realistic manner possible (again, the 'default' way that the model would be used), and to facilitate comparison to observed results. The sites considered have minimal elevation changes, and with the exception of Høvsøre (located 1.5km from the coast), have only minor roughness-changes that do not significantly influence the modelled or measured winds.

From Figure 3 one can see that the new model reduces the absolute error for nearly all extrapolations. The figure also shows enhanced improvement for more drastic extrapolations, though these are less common in practice (as well as in the measurements), as evidenced by the increased bin widths; for example a value of $\ln(z_{\rm rec}/z_{\rm src})$ equal to 2.2 corresponds to extrapolation to 9 times the observation height (which amounts to extrapolating measurements from around 10–15 m to typical hub heights). While there is improvement shown by the new 'tall' model, one can also see that the variability for a given extrapolation distance is appreciably larger than the improvement afforded by the new model.

Results for representative extrapolations at a number of onshore mast sites are shown in Table II, where the 'source' and 'receiver' (target) heights were chosen as those most resembling typical measurement and hub heights at each site. For this first comparison, in the new model we used values of $\{\sigma_\pm, n_+\}$ corresponding to the recommended EWA (default WAsP) parameter values of $\{H_{\rm off}, H_{\rm rms}\}$ over land, as in Figs. 1–2. From the table one sees that the probabilistic model, implemented as described above, gives predictions which tend to be better than those of the current EWA/WAsP method. However, we note that such predictions will be changed when the values of $\sigma_\pm$ are calculated (or adjusted to be representative) for the given sites, giving overall improvement of the new model's predictions as shown in section 3.2.

Site	$z_{\rm src}, z_{\rm rec}$ (m)	$U_{\rm src}$ ($\rm ms^{-1}$)	$U_{\rm rec}$ ($\rm ms^{-1}$)	$U_{\rm rec}^{\rm EWA}$ ($\rm ms^{-1}$)	$U_{\rm rec}^{\rm new}$ ($\rm ms^{-1}$)	$\rm error_{EWA}$ (%)	$\rm error_{new}$ (%)
Høvsøre	60, 116.5	8.67	9.69	9.56	9.63	-1.4	-0.7
Hamburg	50, 175	4.62	6.99	6.61	6.82	-5.5	-2.3
Cabauw	40, 140	5.80	8.03	7.86	7.94	-2.1	-1.1
Risø	43, 117	6.63	7.95	8.17	8.22	2.7	3.4
Kivenlahti	92, 224	5.37	7.35	7.25	7.41	-1.3	0.9

Table II. Extrapolation error at various sites, using available heights $\{z_{\rm src}, z_{\rm rec}\}$ closest to typical measurement and prediction levels.

3.2. Extrapolation including measured flux statistics

For several test sites (Cabauw, Hamburg, Høvsøre), sonic anemometers were part of the instrumentation, giving velocity component, temperature and flux statistics (see e.g. [12] for more details). For these sites, we also did extrapolations using (12) in (18) and (17) with the momentum flux and heat flux statistics, via the stability variability parameters $\sigma_\pm$ calculated as in (4) from 10m-height sonic anemometer measurements at each of these sites. Figure 4 shows the mean absolute error per relative extrapolation $\ln(z_{\rm rec}/z_{\rm src})$, for the new model both using the default values (as in Fig. 3) and using observed flux statistics, compared to the EWA/WAsP model. Note that the bin widths are wider in Fig. 4, because there were less data points in the dataset (3 sites) where $\sigma_\pm$ could be calculated; again the bins were chosen such that each contained the same number of samples.

From Figure 4 one can see that using the stability measurements leads to further improvement of the extrapolations compared to the EWA method, with systematically smaller absolute error per extrapolation distance. There is a minor exception to the general improvement, for extreme extrapolations to at least 10 times measurement height. This is not unexpected, and does not significantly impact use of the new model with flux statistics—addition of surface-layer flux information is not expected to improve extrapolation of surface-layer wind data to heights which may sometimes lie above the ABL and are more directly affected by the capping inversion, and such extrapolation (e.g. from 10–15 m to 100–250 m) is not recommended. For extrapolations of $\ln(z_{\rm rec}/z_{\rm src})\approx$0.4 (about 50% above measurement height), the new model including flux information gives mean absolute errors slightly larger than the EWA model. But, as shown in Figure 5, for extrapolations of $\sim 50\%$ the *mean error* from the new model including fluxes is a bit smaller than those from the EWA. Overall, Fig. 5 shows that the new model using default settings gives mean extrapolation error closer to zero

[‡‡] The 'default' values of $h_{\rm eff}$ over land and sea are chosen to be consistent with the distributions aggregated by Liu and Liang [20], and also give mean wind profile shapes consistent with those observed e.g. by the offshore LIDAR in this study.

than the EWA model, and that using flux observations tends to reduce this error further. We note however, that while an improvement can be seen using the new model, the differences between new and old (EWA/WAsP) tend to be of the same magnitude (or smaller) than the standard deviation per log-extrapolation distance (represented by the bars in Figs. 3– 5).

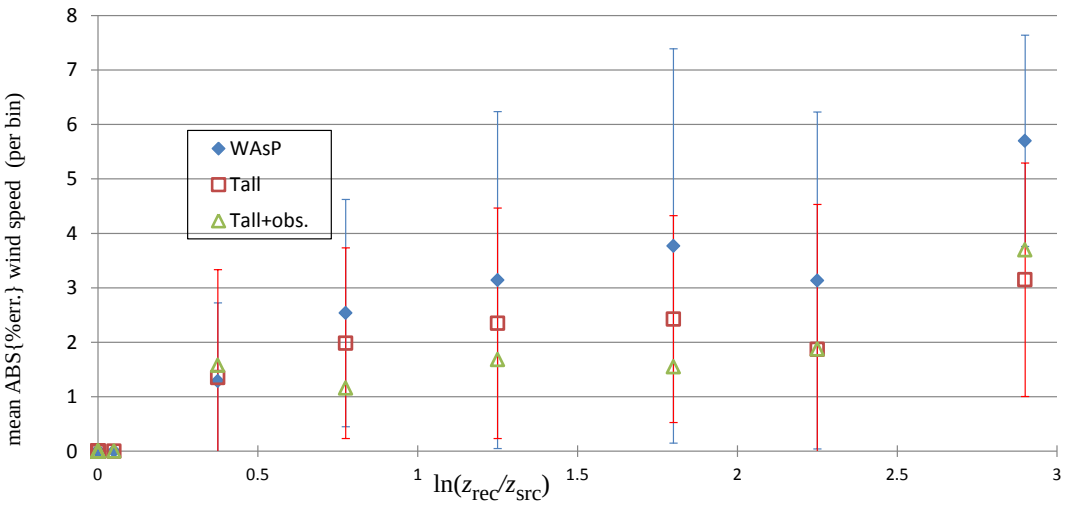

Figure 4. Mean of absolute error in wind speed extrapolation per relative extrapolation bin in $\ln(z_{\rm rec}/z_{\rm src})$, also using measured flux statistics (yellow triangles) instead of the 'default tall' parameters (red squares).

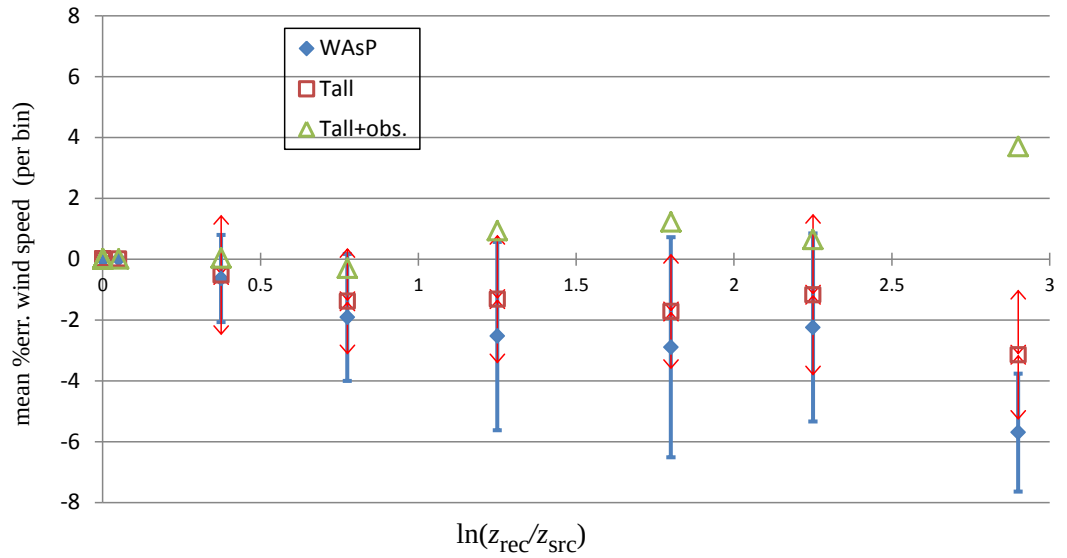

Figure 5. Mean error in wind speed extrapolation per relative extrapolation bin in $\ln(z_{\rm rec}/z_{\rm src})$, also using measured flux statistics (yellow triangles) instead of the 'default tall' parameters (red squares).

The new model with default settings gives smaller standard deviations of absolute error per extrapolation distance than the EWA, as shown in Figure 6 (and by the error bars in the preceding plots); this is also generally true of the new model using observed fluxes, though the added flux information translates into more variability at some extrapolation distances. From the plots using the limited number of sites that include sonic anemometer flux measurements, i.e. Figures 4–5, one might expect little improvement from the new model for more 'conservative' extrapolations to heights less than double the observation height ($\ln[z_{\rm rec}/z_{\rm src}]\lesssim 0.7$); however, the reader is reminded that the full data set here, as seen in Figure 3, shows improvement of the new model over the EWA for such 'typical' extrapolations.

Wind Energ. 2014–2016; **00**:1–15
DOI: 10.1002/we
Prepared using weauth.cls

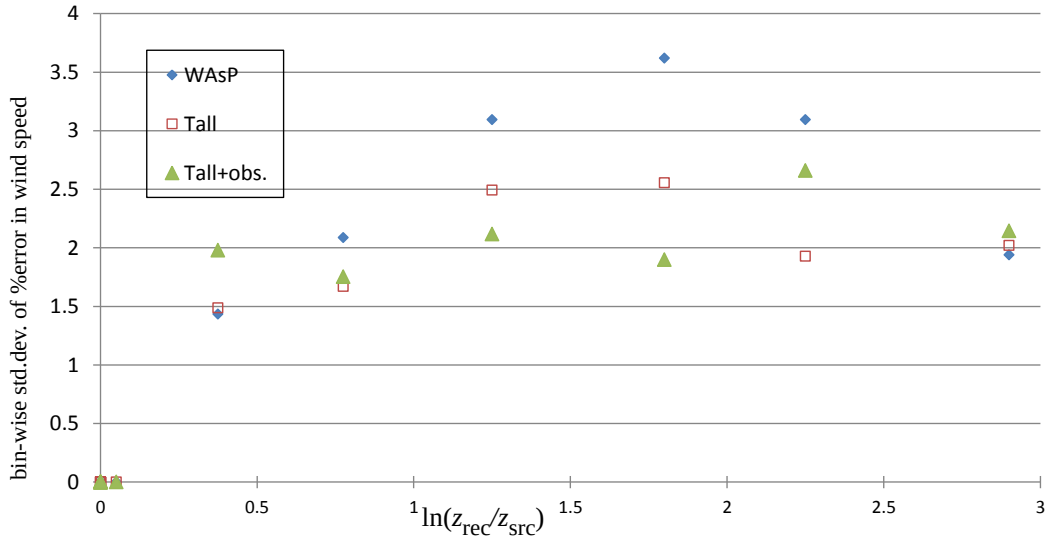

Figure 6. Standard deviation of error in wind speed extrapolation, per relative extrapolation $\ln(z_{\rm rec}/z_{\rm src})$. Colors as in Figs. 4–5.

3.3. Uncertainty in vertical extrapolation

In the previous section we evaluated the performance of the original EWA and new 'tall' vertical extrapolation modelling, but this can also be extended to gauge the uncertainty in the models. Looking at the figures of the previous section, one can see direct correspondence between absolute error in wind speed and relative vertical extrapolation $(z_{\rm rec}/z_{\rm src})$. Considering all the data in this work, i.e. Figure 3, along with the fact that the EWA's perturbation form (13) is dominated by contributions that involve $\ln(z/z_0)$ and z/z_m and this is applied as source-receiver ratios as in Eq. 14, one may expect the extrapolation error to be proportional to some combination of $\ln(z_{\rm rec}/z_{\rm src})$ and $(z_{\rm rec}/z_{\rm src})$. This is also expected when using the adapted 'tall' model as well, due to the logarithmic and linear z-dependences in the climatological profile (11) and associated stability correction (12). Indeed, for extrapolations up to twice a given measurement height, as seen by the linear trend in Figure 3, the absolute error has a behavior of roughly

$$|\%\text{error}|_{z_{\rm rec}<2z_{\rm src}} \approx 0.6\% + c_{\varepsilon 0} \ln\left(\frac{z_{\rm rec}}{z_{\rm src}}\right). \tag{21}$$

We find a proportionality constant $c_{\varepsilon 0}$ of approximately 2% for the EWA model (14–15). For the new tall profile model (11–12) adapted to the EWA perturbation framework (i.e. Eqs. 17–19), the extrapolation error and thus the coefficient in (21) is smaller, $c_{\varepsilon 0} \sim$1.3%, reflecting improved performance and presumably lower uncertainty. Using the EWA (WAsP) framework with either model, one may take (21) as an estimate for the uncertainty for 'typical' extrapolations, i.e. not significantly beyond twice the observation height. For more extreme extrapolations, the mean error deviates from logarithmic. For extrapolations beyond twice the measurement height, the uncertainty could be estimated using a form involving both dependences; e.g. a log-linear form $\sqrt{c_\varepsilon \ln(z_{\rm rec}/z_{\rm src}) + c_{\rm lin}(z_{\rm rec}/z_{\rm src})}$, where $\{c_\varepsilon, c_{\rm lin}\}$ would be roughly $\{4, 0.5\}\%$ for the EWA/WAsP model and $\{2.5, 0.3\}\%$ for the new tall model.

We re-iterate that our uncertainty estimates (and thus Eq. 21) are based on fewer than 15 sites, and that the bin-wise standard deviation (as seen in Fig.6) is nearly as large as the mean absolute error.

4. DISCUSSION AND SUMMARY

Here we have adapted the probabilistic 'tall' dimensionless profile theory of [12] for use within the framework of the European Wind Atlas (EWA) methodology [14], i.e. to be consistent with site-to-site application via the geostrophic drag law. The dimensionless climatological wind profile (5) is a natural choice for extension of the EWA methodology, since it is expressed simply as a logarithmic piece plus terms for the effects of stability and ABL-depth. Using $\langle U/u_{*0}\rangle$ facilitates treatment of 'direct' (e.g. Monin-Obukhov) stability corrections separately from (geostrophic-scale) surface friction velocity perturbations, as in the EWA. We have made a simplification by defining the mean dimensionless wind through integration over the stability distribution $P(L^{-1})dL^{-1}$, effectively simplifying the joint behavior of u_{*0} and L^{-1}. We have also implicitly assumed u_{*0} to be Weibull-distributed—which is an inherent consequence of the form of the first-order EWA treatment as well. The applicability of the stability-based simplification becomes weaker over water, where the

air-sea temperature difference ΔT_{aw} becomes the relevant quantity (as opposed to the near-surface heat flux and L), and where u_{*0} and L^{-1} have a more complicated relationship that may demand 'two-dimensional' treatment, i.e. consideration of the joint probability density $P(\Delta T_{aw}, u_*)$. This is reflected (and practically compensated for) by the σ_+ used over sea in practical implementation (WAsP), which to match the successful EWA surface-layer mean-wind modeling, is set to be smaller than the average σ_+ found from over-sea measurements and mesoscale modelling made thus far (e.g. [26]). Details of the latter are beyond the scope of this work, but progress continues in this area.

To make the dimensionless wind profile amenable for use with the geostrophic drag law (16) applied in the EWA, we retain the mean geostrophic-scale ('offset') heat flux contribution perturbing the (mean) friction velocity, as in the perturbation form of the EWA. This is necessary to account for the effect of heat flux upon the geostrophic balance, whereby the integrated atmospheric boundary-layer momentum transfer (in effect from geostrophic level to the ground) is different than for neutral conditions. For a given G, the neutral value of u_* is in effect perturbed (to first order, see Appendix) by the geostrophic-scale mean heat flux $H_{\rm offset}$, which leads to a height-independent "offset" of the implied long-term mean wind profile. We have normalized the new 'tall' form for dimensionless profile $\langle U/u_{*0}\rangle$ by its logarithmic component, then included the (geostrophic) Δu_{*0} "offset" term in the profile. This normalization, consistent with the EWA form, results in a perturbative mean wind profile expression $(1 + \Delta U/U_0)$ which, while containing terms nonlinear in the height z above ground, does not vary through the ABL as much as the EWA form. That is, the new model has decreasing shear as the climatological effective ABL 'top' is approached, as the mean wind approaches the mean geostrophic value (and the mean direction changes as well, not explicitly represented in the new model). The new adapted wind profile model can be viewed like a perturbation around $z \simeq 0$ (actually z_0), whereas the EWA version is a linear perturbation around $z = z_m$; thus we allay concerns with the new model retaining a geostrophic piece, i.e. the geostrophic-scale "offset" heat flux being affected by the surface-layer shear dU/dz (below z_m). However, the offset term $\Delta u_{*\rm off}$ (and thus $H_{\rm off}$) might be expected to depend slightly on the newly-utilized stability statistics (primarily the effective width $\sim n_+\sigma_+$ of the stability distribution during stable conditions), though this small effect is neglected in the current treatment. Further, to adapt the probabilistically-derived mean wind profile for application from one surface to another, the geostrophic-scale effect of roughness was included in the stability treatment, modeled in a way consistent with the EWA treatment. Doing so involves a low-order model with uncertainty, on par with application of the first-order EWA methodology.

The performance of both the new 'tall' model and the WAsP/EWA 'standard' model for vertical extrapolation was investigated at a significant number of ideal (relatively homogeneous, mostly flat) sites on land and offshore, over a large number of extrapolation distances. Without including measured heat flux statistics, the tall model performed a bit better than the EWA model, though the improvement was not large compared to the variability in extrapolation errors. Guided by the form of the EWA extrapolation model and the extrapolation error results, we suggest a basic form (21) for estimating the uncertainty in vertical extrapolation using the original EWA formulation. Similarly we arrive at the same form for the adapted 'tall' model, with a slightly different constant reflecting the smaller expected error in the new model. We also consider extrapolations at a small number of sites with sonic anemometers measuring fluxes of heat and momentum, using the flux statistics in the new model; inclusion of this information improves the results further over the EWA method, generally compensating (perhaps over-compensating) for the negative bias seen using the EWA method with default settings.

Implications and ongoing work

While the 'tall profile' adaptation and implementation modestly improved results for upward extrapolation of long-term mean wind speed, we point out that for prediction of annual energy production (AEP), one must also use an appropriately modified model for vertical extrapolation profile of the Weibull-k parameter or long-term second-moment of wind speed. The EWA framework includes such a model for Weibull-k and long-term $\langle U^2\rangle$, while a successful 'tall' implementation is currently under development and testing [15].

Continuing work also includes universal characterization of the connection between the distributions of stability $P(L^{-1})$ and shear dU/dz in the surface layer, particularly under stable conditions, to produce useful estimates of the primary profile-impacting parameter σ_+ from measured wind shear statistics. Further concurrent work includes incorporation of expected ABL depth distributions in the theory, including correlation with stability, for improvement of Weibull-k profiles obtained via profiles of long-term higher (e.g. second) moments of the wind speed along with the mean wind. Also under development is a model of the turning of the wind with height (veer), consistent with the probabilistic theory and geostrophic drag-law application.

DOI: 10.1002/we
Prepared using weauth.cls

A. APPENDIX: STABILITY PERTURBATION OF GEOSTROPHIC DRAG LAW AND WIND PROFILE

We provide an updated derivation of geostrophic-scale stability-induced perturbation of the friction velocity (and subsequently logarithmic wind profile around the height of minimum stability-induced deviations, z_m). The derivation is rooted in perturbation of the geostrophic drag law, and leads (with some assumptions) to the stability model of the European Wind Atlas [14]. The derivation is extended to update the parameter relating z_m to the geostrophic wind, latitude, and roughness.

The EWA [14] in effect estimates the geostrophic-scale perturbation $\mathrm{d}u_*$ due to first-order perturbations $\mathrm{d}H$ in geostrophic-scale heat flux (from neutral, i.e. $H = 0$), arising from the stability-dependence of the barotropic geostrophic resistance-law constants A_0 and B_0. We begin by employing the stability parameter $\mu \equiv \kappa(u_*/f)/L$, so to first order in μ we have $\mathrm{d}A = \mathrm{d}\mu(dA_0/d\mu)$ and $\mathrm{d}B = \mathrm{d}\mu(dB_0/d\mu)$. Because $u_*/L = -(\kappa g/T_0)H/u_*^2$, one may write

$$\frac{d\mu}{\mu} = \frac{dH}{H} - 2\frac{du_*}{u_*}, \tag{A.1}$$

i.e. $d\ln\mu = (d\ln H - 2d\ln u_*)$. For a given forcing G and ignoring dz_0, the differential of the geostrophic drag law

$$G = \frac{u_{*0}}{\kappa}\sqrt{\left[\ln\left(\frac{u_*/f}{z_0}\right) - A_0\right]^2 + B_0^2}, \tag{A.2}$$

gives

$$0 = dG = G\frac{du_*}{u_*} + \frac{u_*/\kappa}{\sqrt{[\ln(u_*/fz_0) - A_0]^2 + B_0^2}}\left\{\left(\frac{du_*}{u_*} - dA_0\right)\left[\ln\left(\frac{u_*/f}{z_0}\right) - A_0\right] + B_0 dB\right\}; \tag{A.3}$$

now using $dB_0/d\mu = 0.2 = -dA_0/d\mu$ as in [14], then dividing by G we get

$$0 = \mathrm{d}\ln G = \mathrm{d}\ln u_* + \left(\frac{u_*}{\kappa G}\right)^2\left\{(\mathrm{d}\ln u_* + 0.2\mathrm{d}\mu)\left[\ln\left(\frac{u_*/f}{z_0}\right) - A_0\right] + 0.2B_0\mathrm{d}\mu\right\}. \tag{A.4}$$

Exploiting Eq. A.1 (e.g. $d\mu = \mu\mathrm{d}\ln H$), we can rearrange Eq. A.4 to give a relation between first-order perturbations in geostrophic heat flux and friction velocity,

$$d\ln u_* = \frac{-0.2\left(\frac{u_*}{\kappa G}\right)^2\left\{B_0 + \left[\ln\left(\frac{u_*/f}{z_0}\right) - A_0\right]\right\}}{1 + \left(\frac{u_*}{\kappa G}\right)^2\left\{(1 - 0.4\mu)\left[\ln\left(\frac{u_*/f}{z_0}\right) - A_0\right] - 0.4\mu B_0\right\}}(\mu\, d\ln H). \tag{A.5}$$

But $\mu\,\mathrm{d}\ln H = -(g\kappa^2/u_*^2 f T_0)dH$, and we are perturbing around a neutral state, so that $\mu = 0$ and (A.5) becomes

$$d\ln u_* \simeq 0.2\left\{\ln\left(\frac{u_*/f}{z_0}\right) + B_0 - A_0\right\}\frac{g}{fT_0G^2}dH. \tag{A.6}$$

A form equivalent to $\mathrm{d}\ln u_* = c_G(g/\rho c_p T_0 f G^2)\mathrm{d}H$ is given by the EWA [14] (where the factor ρc_p is for dH given in W/m^2), which is equal to (A.6) but with $0.2\{\ln(u_*/fz_0) + B_0 - A_0\}$ replaced by a constant c_G equal to 2.5.This value falls within the range of effective c_G found via (A.6), for the ranges of u_*, f, and z_0 encountered in practice. For smoother surfaces (z_0 of several cm or less) and appreciable friction velocities the choice of $c_G = 2.5$ gives low du_* compared to (A.6), while rougher surfaces and low friction velocities lead to the opposite result.

One can also interpret the perturbation theory here in terms of the geostrophic-to-surface wind turning (cross-isobaric) angle φ_G; for the ideal case of barotropic boundary layers (i.e. insignificant horizontal gradients of surface temperature) then the conventional relation $\tan\varphi_G = -B_0/[\ln(u_*/fz_0) - A_0]$ applies [27, 28]. The lack of φ_G dependence can be interpreted as a sensible choice in the EWA model, given that the $\tan(\varphi_G)$ dependence is not proper for latitudes approaching the equator [29], and from the EWA's implicit assumption that (in the stability treatment) variations in dH would dominate those do to geostrophic turning. We also remind that near the equator the geostrophic wind becomes ill-defined (the boundary-layer depth implied by $\ln(u_*/f/z_0)$ becomes unphysically large), due to the dominant ABL balance arising not from the Coriolis force but from other mechanisms. However, the geostrophic drag law form is still used with limited success in the tropics, due to the Coriolis parameter being limited in WAsP in such a way that the implied time scale corresponds to that of dominant (diurnal) forcings of the ABL.

A.1. Height of minimum stability-induced perturbations

The scale z_m is defined by the EWA [14] to be where first-order effects of surface heat-flux variations vanish, at a height where the differential of the Monin-Obukhov wind profile is zero:

$$\mathrm{d}\left\{u_*\left[\ln\left(\frac{z}{z_0}\right)-\psi(zL^{-1})\right]\right\}\Big|_{z=z_m}=0.$$

Thus

$$\left[\ln\left(\frac{z_m}{z_0}\right)-\psi\left(z_mL^{-1}\right)\right]du_*-u_*L^{-1}\frac{d\psi}{\mathrm{d}L^{-1}}\left[d\ln H-3\,d\ln u_*\right]\;=\;0. \tag{A.7}$$

Since the stable-side correction function is $\psi_+=-bzL^{-1}$ and consequently $d\psi/dL^{-1}\to -bz$ in the neutral limit ($dL^{-1}\to 0$), then employing the (dominant) stable-side form for ψ and the definition of Obukhov length L, and from (A.6) we arrive at

$$\frac{z_m}{\ln(z_m/z_0)}=\frac{c_G}{b}\frac{u_*^3}{\kappa fG^2}. \tag{A.8}$$

Again from (A.5–A.6) we see that $c_G\simeq 0.2[\ln(u_*/f/z_0)-A_0+B_0]$, with the EWA [14] making a practical choice setting $c_G=2.5$. The EWA continues by using the reduced geostrophic drag law [23]

$$u_{*G}=\frac{0.485G}{\ln(G/fz_0)-A_0} \tag{A.9}$$

to replace $(u_*/G)^3$ in (A.8) with $0.5^3/[\ln(u_*/f/z_0)-A_0]^3$, giving $0.1(G/f)/[\ln(u_*/f/z_0)-A_0]^3$ for the right-hand side of (A.8); finally the EWA approximates the expression for $z_m/\ln(z_m/z_0)$ by using a power law to obtain

$$z_m=\alpha_m z_0\left(\frac{G}{fz_0}\right)^{0.9} \tag{A.10}$$

where $\alpha_m|_{\mathrm{EWA}}$=0.002. But we note that such a choice for α_m implies $b=8$, because the constant of 0.1 derives as an effective approximation of $0.5^3c_G/(\kappa b)$; however, this should be equal to 0.16 for $b=4.7$ and $c_G=2.5$. Thus one should have $\alpha_m=0.003$ for this value of c_G, which corresponds to observed reversal heights for Weibull-k profiles [15], whereas using the EWA value of 0.002 gives z_m between 65–80 m. On the other hand, the value of $c_G>2.5$ implied by (A.6) for small to moderate roughness lengths (i.e. not forest or urban areas) is more consistent with the EWA value of α_m. The difference in reversal height due to α_m has a minor impact on the wind profile, and can in some cases affect annual energy production calculations more than the mean wind profile, due to its role in extrapolation of Weibull-k (discussed in [15]). Note if c_G is changed, then one would need to adjust the values of H_{off} and H_{rms} used in the EWA framework. For mid-latitude, simple sites (e.g. those with moderately small roughnesses considered in [12]), we find that the actual H_{rms} is roughly 30–50% of its EWA-recommended value of 100 Wm^2, consistent with increasing c_G by a factor of 2–3 and also (A.6). This points to the difficulty of assigning a physical meaning to the geostrophic-scale perturbation heat flux H_{rms}; any change of c_G would also demand a change of the 'offset' heat flux H_{off} in WAsP as well.

ACKNOWLEDGEMENTS

The authors would like to thank Søren Ott, Jakob Mann, Hans E. Jørgensen, Brian Ohrbeck Hansen, and Duncan Heathfield for discussions involving this work and its implications.

REFERENCES

1. Monin AS, Obukhov AM. Basic laws of turbulent mixing in the surface layer of the atmosphere. *Tr. Akad. Nauk. SSSR Geofiz. Inst.* 1954; **24**:163–187.
2. Kubik M, Coker P, Barlow J, Hunt C. A study into the accuracy of using meteorological wind data to estimate turbine generation output. *Renewable Energy* 2013; **51**:153–158.
3. IEC 61400–1, Edition 3. *Wind turbine generator systems – Part 1: Safety requirements*. International Electrotechnical Comission: Geneva, Switzerland, 2005.
4. Afzal N. Power-law velocity profile in a turbulent Ekman layer on a transitional rough surface. *Quart. J. Roy. Meteor. Soc.* 2008; **134**:1113–1125.

5. Kelly M, Larsen G, Dimitrov NK, Natarajan A. Probabilistic meteorological characterization for turbine loads. *Journal of Physics: Conference Series* 2014; **524**(1):012 076.
6. Dixon J, Swift R. The dependence of wind speed and Weibull characteristics on height for offshore winds. *J. Wind Engineering* 1984; **8**(2):87–98.
7. Blackadar AK. Implications of a simple two-layer model of the diabatic planetary boundary layer. *Atmos. Ocean. Phys.* 1974; **10**:663–674.
8. Csanady GT. Equilibrium theory of the planetary boundary layer with an inversion lid. *Boundary-Layer Meteor.* 1974; **6**:63–79.
9. Wilson JD, Flesch TK. An idealized mean wind profile for the atmospheric boundary layer. *Boundary-Layer Meteor.* 2004; **110**:281–299.
10. Optis M, Monahan A, Bosveld FC. Moving beyond Monin-Obukhov similarity theory in modelling wind-speed profiles in the lower atmospheric boundary layer under stable stratification. *Boundary-Layer Meteor.* 2014; **153**(3):497–514, doi:10.1007/s10546-014-9953-z.
11. Emeis S, Baumann-Stanzer K, Piringer M, Kallistratova M, Kouznetsov R, Yushkov V. Wind and turbulence in the urban boundary layer—analysis from acoustic remote sensing data and fit to analytical relations. *Meteorol. Z.* 2007; **16**(4):393–406.
12. Kelly M, Gryning SE. Long-term mean wind profiles based on similarity theory. *Boundary-Layer Meteor.* 2010; **136**(3):377–390.
13. Gryning SE, Batchvarova E, Brümmer B, Jørgensen H, Larsen S. On the extension of the wind profile over homogeneous terrain beyond the surface boundary layer. *Boundary-Layer Meteor.* 2007; **124**(2):371–379.
14. Troen I, Petersen EL. *European Wind Atlas*. Risø National Laboratory: Roskilde, Denmark, 1989.
15. Kelly M, Troen I, Jørgensen HE. Weibull-*k* revisited: 'tall" profiles and height variation of wind statistics. *Boundary-Layer Meteor.* 2014; **152**:107–124.
16. Wieringa J. Shapes of annual frequency distributions of wind speed observed on high meteorological masts. *Boundary-Layer Meteor.* 1989; **47**:85–110.
17. Lenschow DH, Mann J, Kristensen L. How long is long enough when measuring fluxes and other turbulence statistics? *J. Atmos. Ocean Technol.* 1994; **11**:661–673.
18. Sathe A, Gryning SE, Peña Diaz A. Comparison of the atmospheric stability and wind profiles at two wind farm sites over a long marine fetch in the north sea. *Wind Energy* 2011; **14**:767–780.
19. Pedersen JG, Kelly M, Gryning SE. The effect of unsteady and baroclinic forcing on predicted wind profiles in large eddy simulations: Two case studies of the daytime atmospheric boundary layer. *Meteorologische Zeitschrift* 2013; **22**:661–674.
20. Liu S, Liang XZ. Observed diurnal cycle climatology of planetary boundary layer height. *J. Climate* November 2010; **23**:5790–5809.
21. Foken T. 50 years of the Monin-Obukhov similarity theory. *16th Symposium on Boundary Layers and Turbulence*, Fundamental studies of turbulence: observations, theory, and models session, Amer. Met. Soc.: Portland, ME, 2004; article 7.1.
22. Carl DM, Tarbell TC, Panofsky HA. Profiles of wind and temperature from towers over homogeneous terrain. *J. Atmos. Sci.* July 1973; **30**(30):788–794.
23. Jensen NO, Petersen EL, Troen I. Extrapolation of mean wind statistics with special regard to wind energy applications. *World climate programme report*, WMO, Geneva, Switzerland 1984. report # WCP-86.
24. Hasager C, Stein D, Courtney M, Pea A, Mikkelsen T, Stickland M, Oldroyd A. Hub height ocean winds over the north sea observed by the NORSEWInD lidar array: Measuring techniques, quality control and data management. *Remote Sensing* 2013; **5**(9):4280–4303.
25. Dellwik E, Mann J, Bingöl F. Flow distortion at a dense forest edge. *Quarterly Journal of the Royal Meteorological Society* 2014; **140**(679):676–686.
26. Peña Diaz A, Hahmann A. Atmospheric stability and turbulence fluxes at Horns Rev–an intercomparison of sonic, bulk and WRF model data. *Wind Energy* 2012; **15**(5):717–731.
27. Zilitinkevich SS, Laikhtman DL, Monin AS. Dynamics of the atmospheric boundary layer. *Izv. Atmos. Ocean Phys.* 1967; **3**:170–191.
28. Hess GD. The neutral, barotropic planetary boundary layer, capped by a low-level inversion. *Boundary-Layer Meteor.* 2004; **110**:319–355.
29. Arya SPS, Wyngaard JC. Effect of baroclinicity on wind profiles and the geostrophic drag law for the convective boundary layer. *J. Atmos. Sci.* 1974; **32**:767–778.